Nano Energy 44 (2018) 111–120

Contents lists available at ScienceDirect

Nano Energy

journal homepage: www.elsevier.com/locate/nanoen

Full paper

Significantly improving cycling performance of cathodes in lithium ion batteries: The effect of Al_2O_3 and $LiAlO_2$ coatings on $LiNi_{0.6}Co_{0.2}Mn_{0.2}O_2$

Wen Liu[a,b], Xifei Li[a,b,*], Dongbin Xiong[b], Youchen Hao[a,b], Jianwei Li[a], Huari Kou[a], Bo Yan[b], Dejun Li[a], Shigang Lu[c,**], Alicia Koo[d], Keegan Adair[d], Xueliang Sun[a,b,d,*]

[a] Tianjin International Joint Research Centre of Surface Technology for Energy Storage Materials, College of Physics and Materials Science, Tianjin Normal University, Tianjin 300387, PR China
[b] Institute of Advanced Electrochemical Energy, Xi'an University of Technology, Xi'an 710048, PR China
[c] R&D Center for Vehicle Battery and Energy Storage, General Research Institute for Nonferrous Metals, Beijing 100088, PR China
[d] Nanomaterials and Energy Lab, Department of Mechanical and Materials Engineering, Western University London, Ontario, Canada, N6A 5B9

ARTICLE INFO

Keywords:
$LiNi_{0.6}Mn_{0.2}Co_{0.2}O_2$
Al_2O_3
$LiAlO_2$
Coating
Lithium ion batteries
Cathode materials

ABSTRACT

$LiNi_{0.6}Co_{0.2}Mn_{0.2}O_2$ (NCM) is a highly potential cathode material for lithium-ion batteries (LIBs). However, its poor rate capability and cycling performance at high cutoff voltages have seriously hindered further commercialization. In this study, we successfully design an ultra-thin lithium aluminum oxide ($LiAlO_2$) coating on NCM for LIBs. Compared to Al_2O_3, the utilization of lithium-ion conducting $LiAlO_2$ significantly improves the NCM performance at high cutoff voltages of 4.5/4.7 V. The study reveals that the $LiAlO_2$-coated NCM can maintain a reversible capacity of more than 149 mA h g^{-1} after 350 cycles with 0.078% decay per cycle. Furthermore, $LiAlO_2$-coated NCM exhibits higher rate capacities [206.8 mA h g^{-1} at 0.2 C (50 mA g^{-1}) and 142 mA h g^{-1} at 3 C] than the Al_2O_3-coated NCM (196.9 mA h g^{-1} at 0.2 C and 131.9 mA h g^{-1} at 3 C). Our study demonstrates that the ultra-thin $LiAlO_2$ coating is superior to Al_2O_3 and significantly improves the capacity retention and rate capability of NCM for LIBs.

1. Introduction

The increasing demand for high energy and power density lithium-ion batteries (LIBs) has stimulated great research interest in high performance cathode materials for application in electric vehicles (EVs) and hybrid electric vehicles (HEVs) [1–7]. Among the various cathode candidates, $LiNi_{1-x-y}Co_xMn_yO_2$ materials have displayed several advantages including low cost, high capacity, improved cycling stability, and enhanced safety performance [8–10]. Within this system, nickel-rich layered $LiNi_{0.6}Co_{0.2}Mn_{0.2}O_2$ (NCM) displays good Li-ion diffusivity with minimal temperature dependence [11], as well as a higher specific capacity than both $LiNi_{0.3}Co_{0.3}Mn_{0.3}O_2$ and $LiNi_{0.5}Co_{0.2}Mn_{0.3}O_2$. As a result, NCM has been recognized as one of the most promising cathode materials for application in high performance LIBs [11,12]. However, NCM exhibits several limitations, including poor rate capability and insufficient capacity retention, especially at high cutoff voltages [13]. These challenges are a result of: (i) structural instability originating from the surface sites and distortion of the rhombohedral phase due to the migration of transition metal ions into Li^+ vacant sites, leading to the formation of spinel-like structures and electrochemically inert NiO-like phases [13–15]; (ii) dissolution of metal ions in $LiPF_6$-based electrolytes due to HF corrosion [16,17]; and (iii) electrolyte decomposition at the cathode and subsequent formation of a solid electrolyte interphase (SEI) layer, resulting in increased surface impedance [18]. These challenges greatly hinder practical application in LIBs [17].

To address these challenges, various techniques such as surface modification [19], elemental doping [20], and concentration gradient structures [21] have been utilized to enhance the electrochemical performance of NCM cathode materials. Previously, surface modification has been shown to significantly improve the performance of electrode materials [16,22]. Inorganic compounds such as metal oxides (SiO_2 [23], Co_3O_4 [24], MoO_3 [25], ZrO_2 [26], ZnO [27], CeO_2 [28], and Al_2O_3 [26,29,30]), fluorides (AlF_3 [31]), and phosphates ($Mn_3(PO_4)_2$ [32]) have been coated onto $LiNi_{1-x-y}Co_xMn_yO_2$ to improve the structural stability between the active materials and electrolytes. For example, Co_3O_4-coated $LiNi_{0.6}Co_{0.2}Mn_{0.2}O_2$ was reported to deliver a capacity ranging from 186.5 mA h g^{-1} to 114.1 mA h g^{-1} in the first 100 cycles [24], and the Al_2O_3-coated $LiNi_{0.5}Co_{0.2}Mn_{0.3}O_2$ revealed higher capacity retention of 85% after 100 cycles, in comparison to the pristine electrode (only 75%) [29]. Among these compounds, metal

* Corresponding author at: Institute of Advanced Electrochemical Energy, Xi'an University of Technology, Xi'an 710048, PR China.
** Corresponding author
E-mail addresses: xfli2011@hotmail.com (X. Li), lusg8867@163.com (S. Lu), xsun9@uwo.ca (X. Sun).

https://doi.org/10.1016/j.nanoen.2017.11.010
Received 8 October 2017; Received in revised form 3 November 2017; Accepted 4 November 2017
Available online 21 November 2017

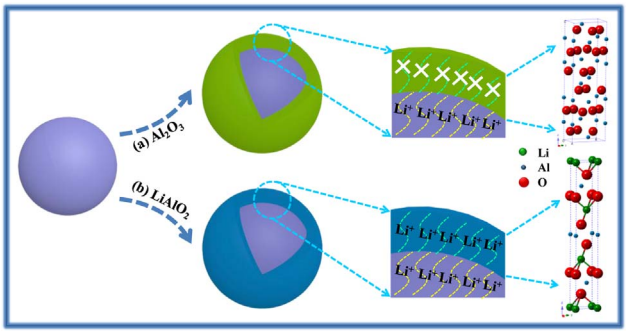

Scheme 1. The difference of two coatings on NCM: (a) metal oxide and (b) solid state electrolyte.

oxides, especially Al_2O_3, effectively prevent the electrode surface from contacting the organic electrolyte, thus alleviating electrolyte decomposition [29]. However, an Al_2O_3 coating may also suppress lithium-ion transfer at the electrode interface, thereby limiting battery performance [17,33]. In contrast, $LiAlO_2$ coatings are well known as lithium-ion conductors [33–35] and have greater lithium diffusivity than Al_2O_3 [33,36]. It has attracted great attention, such as $LiAlO_2$-inlaid $LiNi_{0.5}Co_{0.2}Mn_{0.3}O_2$ exhibiting a better electrochemical performance than the pristine one [37]. These properties enable $LiAlO_2$ to overcome the limited lithium-ion conductivity of metal oxide coatings (Scheme 1) and increase $LiNi_{0.6}Co_{0.2}Mn_{0.2}O_2$ performance in LIBs. To the best of our knowledge, few reports focus on the effect of $LiAlO_2$ coatings on $LiNi_{0.6}Co_{0.2}Mn_{0.2}O_2$ cathode materials at high cutoff voltages of 4.5/4.7 V.

In this study, both Al_2O_3 and $LiAlO_2$ coatings were successfully designed on NCM cathodes for LIBs. Notably, the significant effects of the two coatings on the structural and electrochemical performance of NCM were addressed at high cutoff voltages of 4.5/4.7 V. The resulting structures and electrochemical behavior were discussed in detail.

2. Experimental

2.1. Material synthesis

Commercial NCM was utilized as the cathode material to study the effects of Al_2O_3 and $LiAlO_2$ coatings on battery performance. Both coatings were synthesized via a sol-gel process. $LiAlO_2$-coated NCM was produced by mixing NCM, aluminum(III) sec-butoxide [$Al(sec\text{-}OC_4H_9)_3$, 97%, Aladdin], ethyl acetoacetate (EAcAc), ultrapure water, and ethanol. Lithium methoxide (LiOMe, 98%, Aladdin) was added to the mixture, and stirred continuously at room temperature. The afforded mixture was transferred into a Teflon-lined autoclave and maintained at 150 °C for 15 h. The product was washed with ethanol and subsequently dried in an oven at 80 °C for 4 h. The blend was then collected and calcined. Concentrations of 0.125, 0.25, 0.60, 1.25, 2.5, and 12.5 mol% of $LiAlO_2$-coated NCM were synthesized using this method. These were labelled as Li-Al-O-1, Li-Al-O-2, Li-Al-O-3, Li-Al-O-4, Li-Al-O-5, and Li-Al-O-6, respectively. Similar concentrations of Al_2O_3-coated NCM were synthesized using the above method without the addition of LiOMe and labelled as Al-O-1, Al-O-2, Al-O-3, Al-O-4, Al-O-5, and Al-O-6, respectively.

2.2. Material characterization

The phase of each sample was identified by X-ray diffraction (XRD, Bruker AXS D8Advance). Particle size distribution was estimated from low-angle laser light scattering (LALLS) measurements (Malvern Mastersizer 3000). The sample morphologies and microstructures were analyzed by scanning electron microscopy (SEM, Hitach SU8010) and transmission electron microscopy (TEM, JEOL JEM-3000F). Moreover, energy dispersive X-ray spectroscopy (EDS) mapping was carried out using OXFORD 7426 as the SEM attachment, with an acceleration voltage of 20 kV. Elemental composition information was elucidated using X-ray photo-electron spectroscopy (XPS, VG ESCALAB MK II).

2.3. Electrochemical measurements

CR2032 coin cells were utilized to study the electrochemical performance of the cathode materials. The cathode electrode comprised 80 wt% active material, 10 wt% acetylene black and 10 wt% PVDF binder. Lithium metal foil was used as anode. $LiPF_6$ (1 M) in a 1:1:1 (v/v/v) dimethyl carbonate (DMC)/ethyl methyl carbonate (EMC)/ethylene carbonate (EC) was used as electrolyte. Cell assembly was carried out in a dry argon-filled glove box. Electrochemical tests were carried out using an automatic galvanostatic charge/discharge unit (LAND CT2001A battery tester) between 2.7 and 4.5/4.7 V (versus Li/Li^+) at room temperature. Cyclic voltammetry (CV) tests were performed on a Princeton Applied Research VersaSTAT 4 electrochemical workstation at a scan rate of 0.1 mV s^{-1} and a potential range of 2.7–4.5 V (vs. Li/Li^+). Electrochemical impedance spectroscopy (EIS) was conducted on a Princeton Applied Research VersaSTAT 4 electrochemical workstation, using 2-electrode cells (amplitude voltage is 5.0 mV, and frequency range, 10 mHz–100 kHz).

3. Results and discussion

As shown in Fig. 1(i), the NCM XRD diffraction peaks exhibit sharp and well defined Bragg lines corresponding to a hexagonal α-$NaFeO_2$ structure (space group *R*-3*m*). The XRD patterns of Al-O-1, Li-Al-O-1, Al-O-4, Li-Al-O-4, Al-O-6 and Li-Al-O-6 are compared in Fig. 1(ii)–(vii). All diffraction peaks in the XRD patterns are indexed on the basis of a

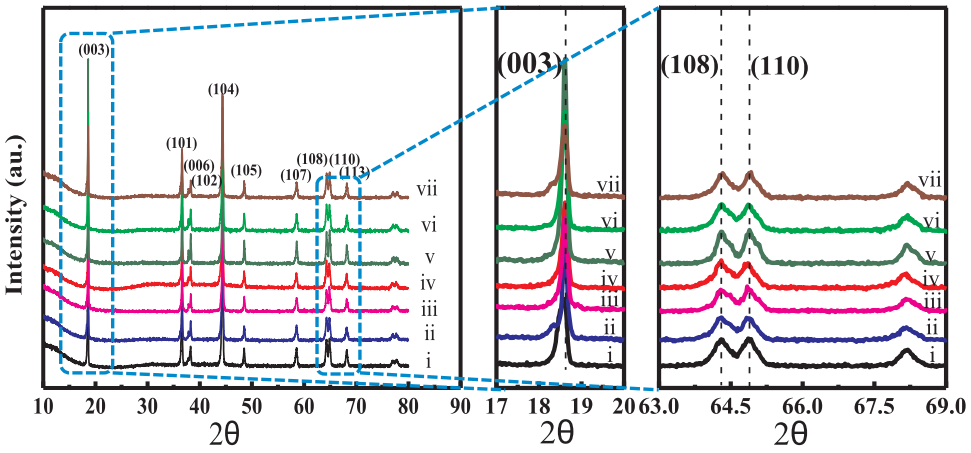

Fig. 1. XRD patterns of (i) NCM, (ii) Al-O-1, (iii) Li-Al-O-1, (iv) Al-O-4, (v) Li-Al-O-4, (vi) Al-O-6 and (vii) Li-Al-O-6.

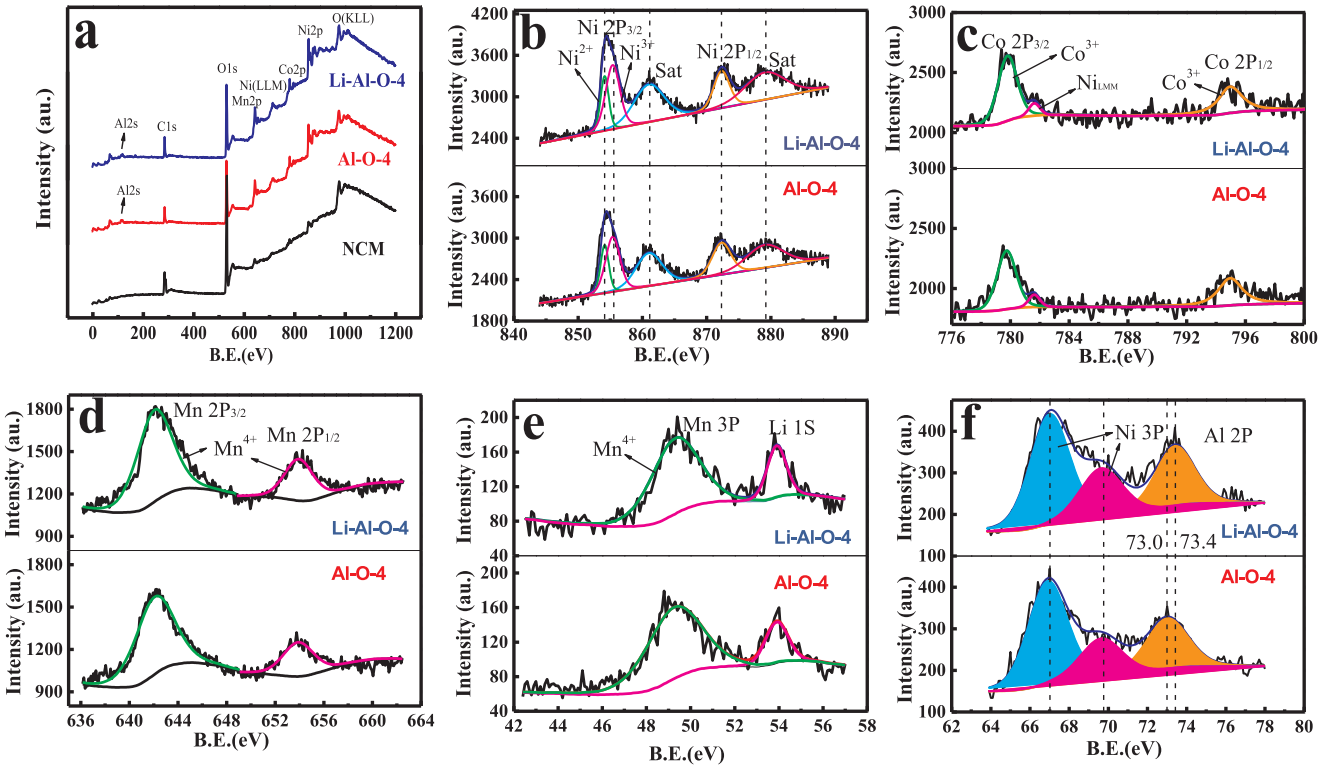

Fig. 2. XPS spectra and fitting results of Al-O-4 and Li-Al-O-4: (a) original XPS survey spectra, (b) nickel spectra, (c) cobalt spectra, (d) manganese spectra, (e) lithium spectra, (f) aluminum spectra.

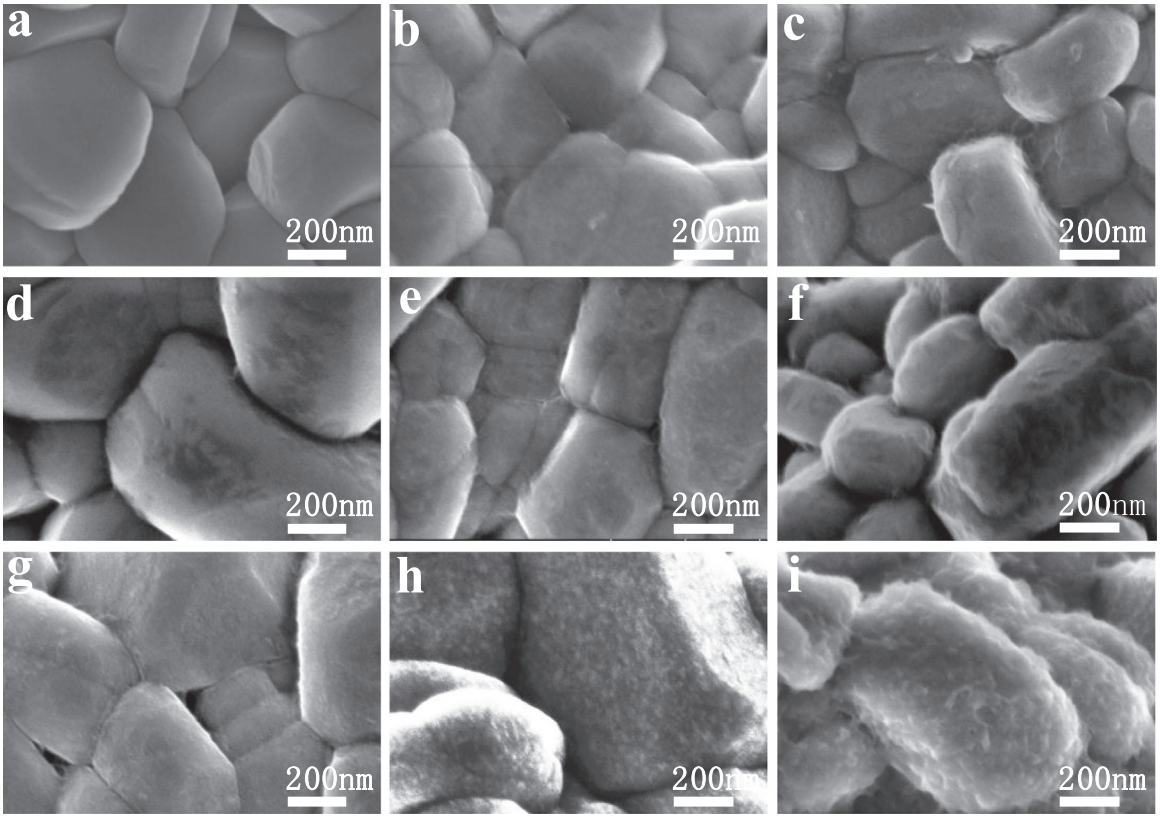

Fig. 3. SEM images of (a) NCM, (b) Al-O-2, (c) Li-Al-O-2, (d) Al-O-4, (e) Li-Al-O-4, (f) Al-O-5, (g) Li-Al-O-5, (h) Al-O-6 and (i) Li-Al-O-6.

hexagonal α-$NaFeO_2$ layered structure without obvious impurities. No peak shifts are observed in the XRD patterns of the coated NCM, indicating the absence of expansion and contraction due to the Al_2O_3 and $LiAlO_2$ coatings. The distinct splitting of the (006)/(102) and (108)/(110) peaks of all the samples demonstrates that these materials have a well-developed layered structure [31]. This suggests that the NCM crystal structure is not affected by the coating layers. Notably, the diffraction peaks corresponding to the Al_2O_3 and $LiAlO_2$ coating layers are absent in Fig. 1(ii)–(vii). This may stem from the amorphous structure of the coating or the coating layer being beyond XRD resolution.

The surface composition and the oxidation states of Ni, Co, Mn, and Al found in Al-O-4 and Li-Al-O-4 (Fig. 2) were elucidated by XPS analysis. The Ni XPS spectra in Fig. 2b display a Ni $2p_{1/2}$ main peak at 872.3 eV with a satellite peak at 879.1 eV. The peaks of the Ni $2p_{3/2}$ spectrum located at 854.1 and 855.4 eV with a satellite peak at 816.0 eV were assigned to Ni^{2+} and Ni^{3+}, respectively. Ni was a mixture of +2 and +3 valence states, and the afforded value of each peak is close to those reported in previous studies [16,38]. The Co XPS spectra in Fig. 2c display a Co $2p_{3/2}$ main peak at 779.8 eV with a Ni (LMM) peak at 781.6 eV and a Co $2p_{1/2}$ main peak at 795.0 eV [39]. These results indicate that there is no change in the valence states of Co in either of the Al-O-4 and Li-Al-O-4 surfaces. Fig. 2d presents the XPS spectra for Mn 2p in which two broad main peaks are observed at 642.1 and 653.9 eV, attributed to Mn $2p_{3/2}$ and Mn $2p_{1/2}$, respectively [16,39]. The results indicate that in the crystal lattice, Mn is mainly in +4 valence state [16,39]. This is consistent with the results in Fig. 2e [40]. Data from Mn XPS analysis also demonstrate that there is no change in the valence state of Mn in Al-O-4 and Li-Al-O-4. The Al $2p_{3/2}$ spectrum demonstrates a binding energy at ~73 eV with trivalent Al (Fig. 2f). Importantly, the Al 2p spectra of Li-Al-O-2 shift to a higher binding energy in accordance with previous results reported for $LiAlO_2$ coating [33]. These XPS results indicate that $LiAlO_2$ was successfully coated onto NCM.

The NCM particles (Fig. S1) display a narrow size distribution with an average diameter of 12.2 μm. The SEM images of NCM, Al_2O_3-coated NCM and $LiAlO_2$-coated NCM are compared in Fig. 3. Contrary to the smooth and clean NCM surface (Fig. 3a), the surface morphologies of both the Al_2O_3- and $LiAlO_2$-coated NCM exhibit a rough surface morphology, especially with an increase in coating content. EDS mapping was carried out to further identify of Al_2O_3 and $LiAlO_2$ distribution on NCM surface. The elemental mappings of Ni, Co, Mn, O, and Al in Fig. 4 reveal that these elements are homogeneously distributed in the selected region, indicating that Al_2O_3 and $LiAlO_2$ are homogeneously coated on the NCM microspheres. Fig. 5a and b present HRTEM images of Al-O-4 and Li-Al-O-4. Interplanar distances of 0.21 nm and 0.48 nm correspond to the (104) and (003) crystal planes of NCM with a hexagonal layered crystal structure [41]. This data is consistent with the XRD results. It is apparent that approximately 1 nm-thick layers of Al_2O_3 and $LiAlO_2$ were deposited onto the NCM.

The initial charge/discharge profiles of NCM, Al-O-2 and Li-Al-O-2 at a current density of 0.2 C (50 mA g^{-1}) in a voltage range of 2.7–4.5 V are presented in Fig. 6a. It can be seen clearly that all three materials reveal similar profiles in the initial charge/discharge processes. A lack of distinct differences indicates that the coating process does not hinder lithium-ion insertion/extraction at the cathode material. The initial charge/discharge capacities of NCM, Al-O-2 and Li-Al-O-2 are 223.6/187.2 mA h g^{-1}, 228.4/196.9 mA h g^{-1} and 242.6/206.8 mA h g^{-1}, respectively, while their initial coulombic efficiencies are 83.7%, 86.2% and 85.2%, respectively. In the initial cycle, the discharge capacity and NCM coulombic efficiency can be enhanced by an appropriate amount of Al_2O_3 and $LiAlO_2$ coating.

To further understand the electrochemical behavior of the electrode materials, the cyclic voltammograms of NCM, Al-O-2 and Li-Al-O-2 were recorded at 2.7–4.5 V at a scan rate of 0.1 mV s^{-1} (Fig. 6b–d). The redox peak of the three samples shows similar shape, indicating that Al_2O_3 and $LiAlO_2$ coating layers do not affect the electrochemical reaction of NCM. Compared to NCM, both the coated NCM samples exhibit a smaller difference in oxidation peaks for the peak positions in the first two cycles, indicating that Al-O-2 and Li-Al-O-2 exhibit less irreversible capacity. In addition, the first two cathodic peaks of Li-Al-O-2 and Al-O-2 corresponding to the Ni^{2+}/Ni^{4+} redox reaction are observed at 3.85/3.82 V and 3.85/3.80 V, respectively. It is worth mentioning that in Fig. 6d the potential gap of Li-Al-O-2 (0.02 V) between the first two cathodic peaks is smaller than that of Al-O-2 (0.05 V), implying that the reversibility of the electrochemical reactions is enhanced in $LiAlO_2$.

The discharge curves of NCM, Al-O-2 and Li-Al-O-2 between 2.7 and 4.5 V at a current density of 0.2 C are compared in Fig. 7. Upon cycling, the NCM discharge capacity (Fig. 7a) decreases at a faster rate than those of Al-O-2 (Fig. 7b) and Li-Al-O-2 (Fig. 7c). Moreover, as the number of cycles increase, the NCM discharge potential decreases greatly with large electrochemical polarization, while those of Al-O-2 and Li-Al-O-2 exhibit an improved trend. As illustrated in Fig. 7d, both the Al_2O_3 and $LiAlO_2$ coatings play a central role in suppressing electrochemical polarization, while Al_2O_3 and $LiAlO_2$ cause a similar effect on electrochemical polarization during the charge/discharge processes. Notably, Li-Al-O-2 maintains a higher capacity, which suggests that $LiAlO_2$ displays a better effect on NCM. These results indicate that the coating strategies may suppress the interfacial reaction between the cathode materials and electrolyte, reducing the interfacial resistance. This is further supported by the EIS results in this study. Moreover, it is clear that $LiAlO_2$ is a better coating material with certain specific property for LIBs.

The cycling stabilities of NCM, Al-O-2 and Li-Al-O-2 were measured at a rate of 0.2 C in a potential window ranging from 2.7 to 4.5 V (Fig. 8a). The uncoated NCM sample exhibits capacity fade, from 187.2 mA h g^{-1} to 149.3 mA h g^{-1} with a capacity retention of only 79.7% after 100 cycles. On the other hand, the Al-O-2 and Li-Al-O-2 have capacity retention values of 84.5% (from 196.9 mA h g^{-1} to 166.4 mA h g^{-1}) and 87.0% (from 206.8 mA h g^{-1} to 179.9 mA h g^{-1}), respectively. These results clearly demonstrate that the optimized $LiAlO_2$ coatings can improve the cycling stability of NCM by protecting the cathode from reacting with the electrolyte and reducing the interfacial resistance between them, while facilitating lithium-ion diffusion. The long-term stability of NCM, Al-O-2 and Li-Al-O-2 is further compared in Fig. 8e. The uncoated NCM reveals the worst cycling performance with 0.20% decay per cycle. For Al-O-2, the capacity drops to < 149 mA h g^{-1} after 200 cycles with 0.12% decay per cycle, while the Li-Al-O-2 maintains a reversible capacity > 149 mA h g^{-1} after 350 cycles with 0.078% decay per cycle. These results suggest that the cycling performance of the cathode materials improves with Al_2O_3 and $LiAlO_2$ coatings (Fig. 8e). Surprisingly, the Coulombic efficiency of Li-Al-O-2 was maintained at 99% after 350 cycles, indicating that the coating strategy of $LiAlO_2$ coating onto NCM is significantly efficient. Although the Al_2O_3 coating delivers stable electrochemical properties with reduced contact area between the active material and the electrolyte, with an increase in coating content, the Al_2O_3-coated NCM rate capability reveals even worse than that observed for the pristine NCM (Fig. S3c). This may be due to the thick layer of Al_2O_3 coating that inhibits lithium-ion diffusion. For the $LiAlO_2$ coating, the inhibitory effect is relatively small (Fig. S3b and d) and Li-Al-O-2, Li-Al-O-4, and Li-Al-O-6, all display improved battery performance compared to NCM. The rate capabilities of the NCM, Al-O-2 and Li-Al-O-2 electrodes are presented at various C-rates between 2.7 and 4.5 V (vs. Li/Li^+) in Fig. 8b. The cells are first charged and discharged at 0.1 C for three cycles, followed by cycling at 0.2 C, 0.5 C, 1 C, 2 C, 3 C, 0.5 C and 0.2 C for every five cycles, respectively. The discharge capacities of NCM, Al-O-2 and Li-Al-O-2 electrodes decrease with increasing current densities. It can be seen that the Al-O-2 and Li-Al-O-2 present better rate capabilities than NCM, especially at high C-rates. Moreover, compared to Al-O-2, the utilization of $LiAlO_2$ as a coating

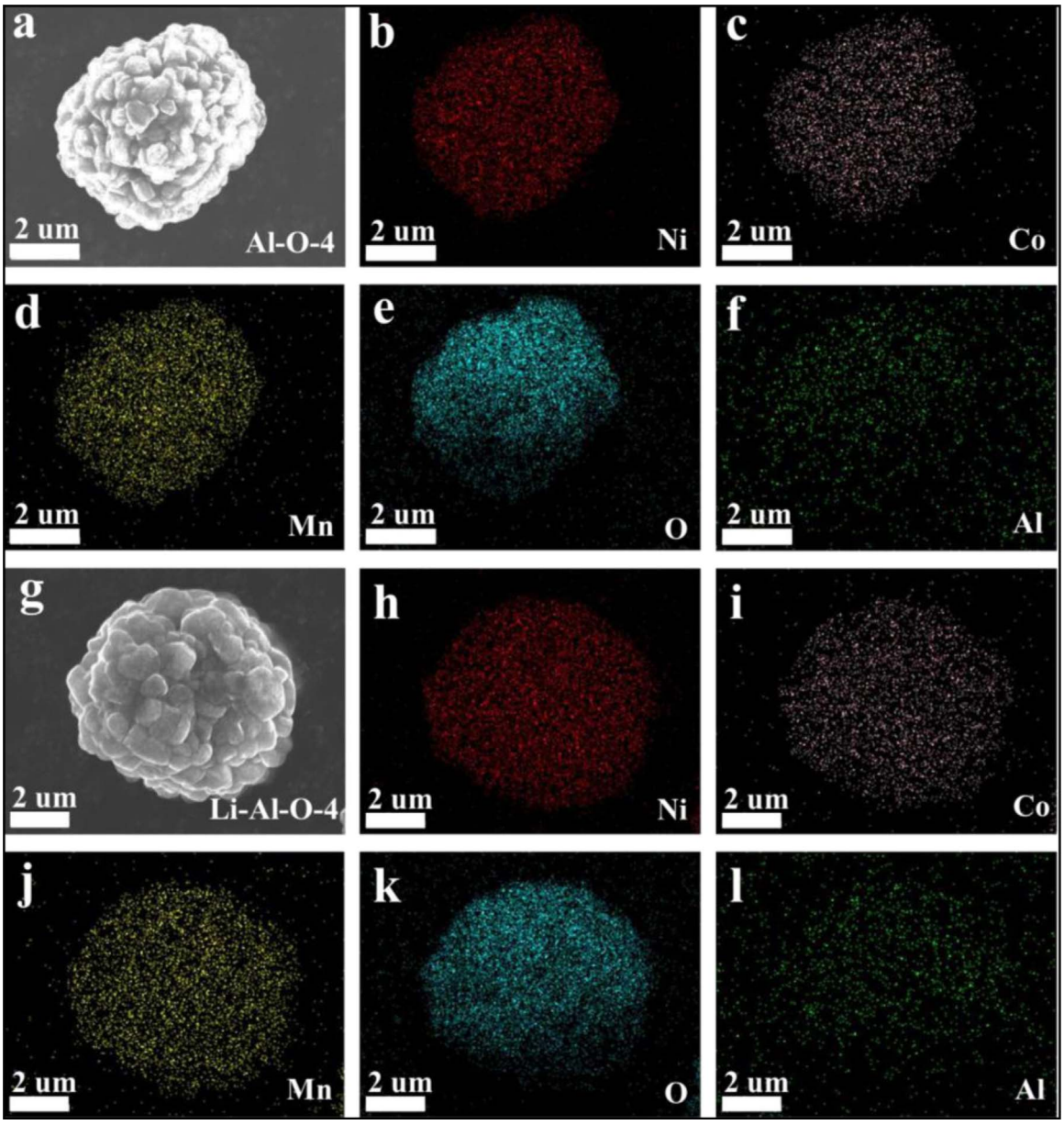

Fig. 4. The comparison of EDS mappings of Al-O-4 and Li-Al-O-4.

material effectively improves the electrochemical performance of NCM at a high cutoff voltage of 4.7 V (Fig. 8c and d). The superior electrochemical performance of Li-Al-O-2 is further confirmed by stabilization of the average discharge voltage when the battery is discharged at half the total capacity, especially at high cutoff voltages and current densities, as presented in the insets in Fig. 8b and d.

As a lithium ion conductor, $LiAlO_2$ interfacial coatings have a positive effect on the transfer of lithium ions to the surface of NCM electrodes [33]. To confirm this, NCM, Al-O-2 and Li-Al-O-2 were investigated via CV analysis at various scan rates. Based on the

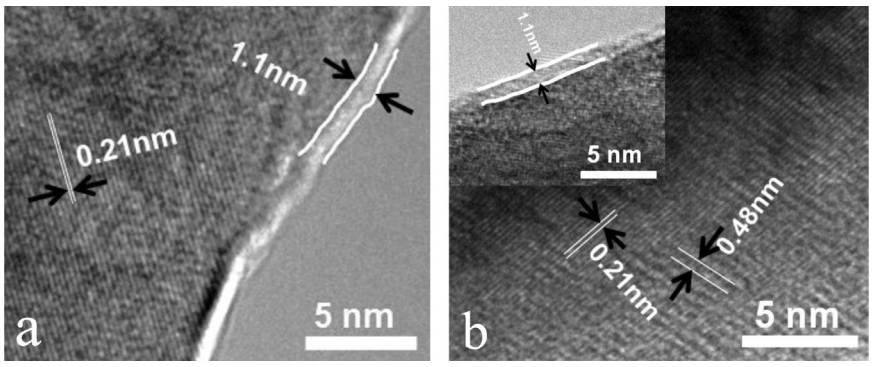

Fig. 5. HRTEM images of (a) Al-O-4 and (b) Li-Al-O-4.

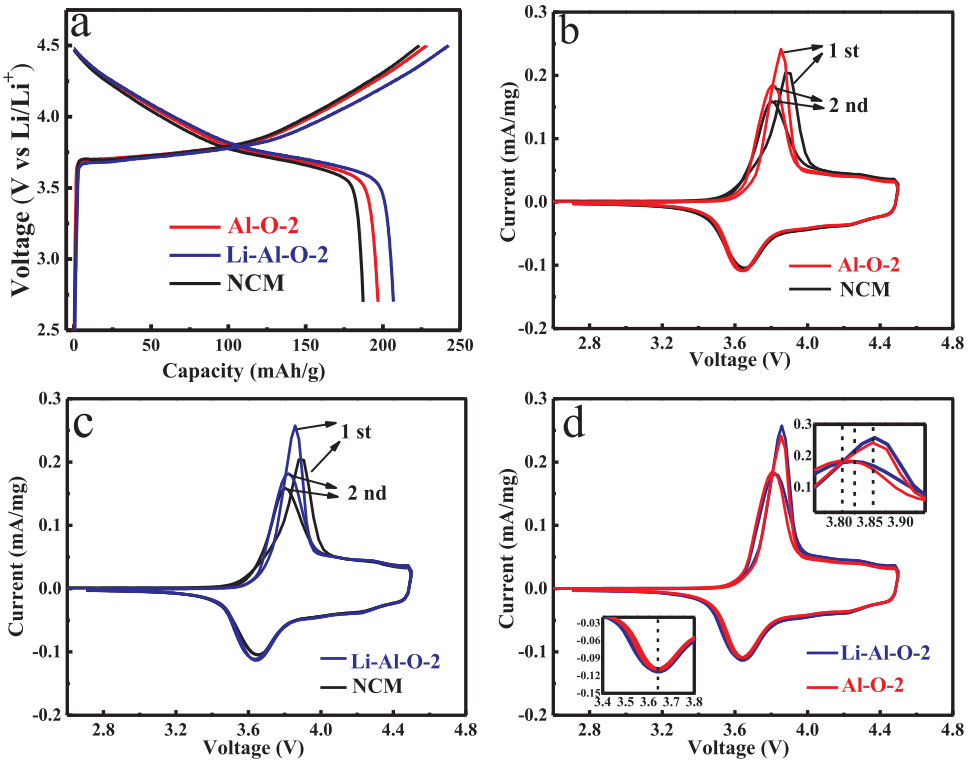

Fig. 6. (a) The initial charge/discharge curves of NCM, Al-O-2 and Li-Al-O-2; the comparison of CV curves at a scan rate of 0.1 mV s^{-1}: (b) NCM and Al-O-2, (c) NCM and Li-Al-O-2, (d) Al-O-2 and Li-Al-O-2.

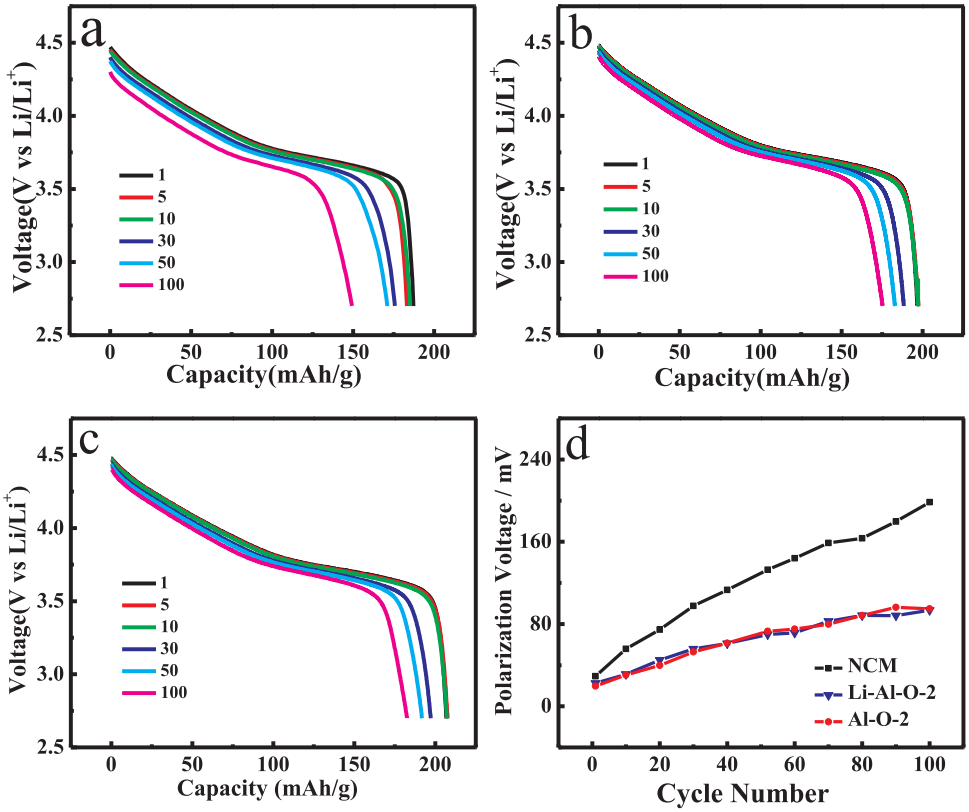

Fig. 7. Galvanostatic discharge profiles of (a) NCM, (b) Al-O-2, and (c) Li-Al-O-2; (d) the electrochemical polarization voltage of NCM, Al-O-2, and Li-Al-O-2.

relationship of the CV scan rates ($\nu^{1/2}$) versus the peak current (I_p), the lithium-ion diffusion coefficient of NCM, Al-O-2 and Li-Al-O-2 may be calculated as follows:

$$I_p = 2.69 \times 10^5 \times n^{3/2} \times A \times D^{1/2} \times \nu^{1/2} \times C_0 \quad (1)$$

where n is the number of electrons in the specific electrochemical reactions, A is the electrode area (cm^2), D is the diffusion coefficient of lithium, ν is the potential scan rate (V s^{-1}), and C_0 is the initial concentration of Li-ion in the cathode (mol cm^{-3}) [42]. Due to the effects of polarization and irreversible behaviors, the anodic peaks shift to higher potentials, while the corresponding cathodic peaks move to lower values [43–45]. The fitting results of the NCM, Al-O-2 and Li-Al-

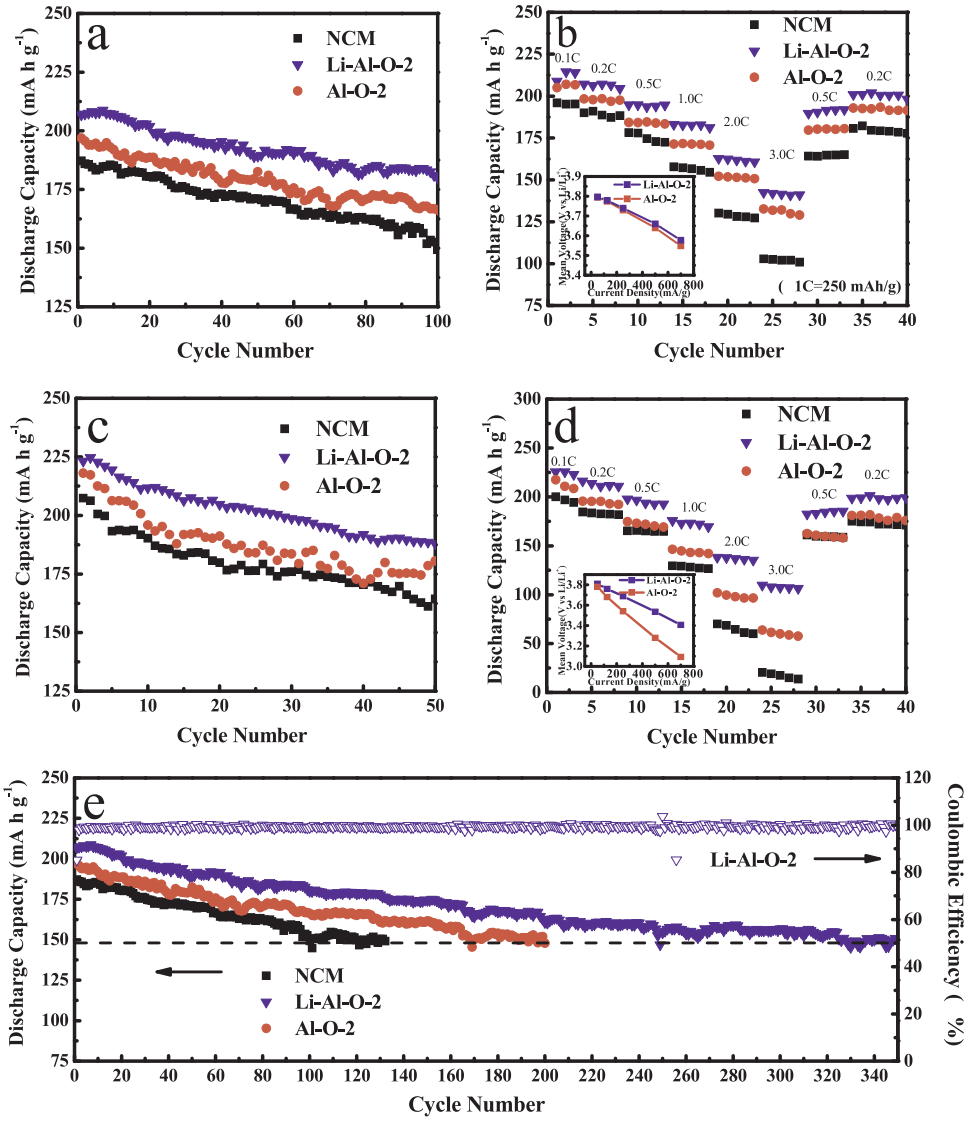

Fig. 8. (a) Cycle performance of NCM, Al-O-2, and Li-Al-O-2 at a rate of 0.2 C (50 mA g^{-1}) in a voltage range of 2.7–4.5 V vs. Li/Li^+; (b) rate capability of NCM, Al-O-2, and Li-Al-O-2 at various current densities in the range of 25–750 mA g^{-1} in a voltage range of 2.7–4.5 V vs. Li/Li^+; (c) cycle performance of NCM, Al-O-2, and Li-Al-O-2 at a current density of 0.2 C in a voltage range of 2.7–4.7 V vs. Li/Li^+; (d) rate capability of NCM, Al-O-2, and Li-Al-O-2 at various current densities in the range of 25–750 mA g^{-1} in a voltage range of 2.7–4.7 V vs. Li/Li^+. (e) The comparison of cycle performance of NCM, Al-O-2, and Li-Al-O-2 with an electrochemical window of 2.7–4.5 V vs Li/Li^+.

O-2 electrodes are presented in Fig. 9a–c. For all three electrodes, the redox peak currents (i_p) exhibit a linear relationship with the square root of the scan rate ($\nu^{1/2}$) that originates from the diffusion-limited intercalation/deintercalation processes of the lithium ions. Both coating materials reveal a different effect on lithium-ion diffusion. Based on Eq. (1), the value of lithium-ion diffusion ($D_{Li}{}^+$) was calculated for NCM, Al-O-2, and Li-Al-O-2 as summarized in Table 1. $D_{Li}{}^+$ value of Li-Al-O-2 is higher than those of NCM and Al-O-2, indicating that the $LiAlO_2$ coating layer improves lithium-ion diffusion during the extraction/insertion processes. Additionally, the improved Li^+ diffusion originated from $LiAlO_2$ coating may inhibit the formation of NiO-like phases on the NCM surface, which may reduce the interfacial resistance between the cathode and electrolyte. Therefore, the $LiAlO_2$ coating can better improve the rate capability of the cathode materials.

To further investigate the possible reasons for enhanced performance of the Al_2O_3- and $LiAlO_2$-coated NCM, EIS was performed at a discharged state of 4.0 V in the frequency range from 1 mHz to 100 kHz, as represented in Fig. 10. Each of the resulting impedance spectra comprises three regions: (i) a semicircle in the high frequency region related to the interfacial film resistance [solid electrolyte interface (SEI)]; (ii) a semicircle at the intermediate frequency region representing the charge interfacial capacitance and transfer resistance at the electrode/electrolyte interface; (iii) a sloping line at the low frequency region associated with the Warburg impedance representing lithium-ion diffusion through the solid electrode [18,40,46]. In the equivalent circuit as shown in Fig. 10c, R_s represents the resistance of the electrolyte solution, R_f is the resistance of the surface SEI film, R_{ct} corresponds to the charge transfer resistance, CPE is the capacitance of the electrode/electrolyte double layer, and W_1 represents the Warburg impedance. All the impedance spectra were fitted with the equivalent circuit to calculate the values of R_s, R_f, and R_{ct}, as listed in Table 2. Notably, the R_s values for NCM, Al-O-2 and Li-Al-O-2 are similar, suggesting that neither coating dissolves in the electrolyte to affect the solution composition and conductivity. Furthermore, the R_{f+ct} value increase upon subsequent cycling. In comparison, the initial NCM R_{f+ct} value increases from 181.1 to 449.4 after 30 cycles, whereas those of Al-O-2 and Li-Al-O-2 increase from 121.5 to 283.4 and from 71.1 to 149.2, respectively. The R_{f+ct} of Al-O-2 and Li-Al-O-2 are significantly smaller than that of NCM. This data suggests that the Al_2O_3 and $LiAlO_2$ coating layers can suppress the interface side reactions between the cathode and electrolyte to reduce the interfacial resistance. Moreover, Li-Al-O-2 has a smaller R_{f+ct} value than Al-O-2, probably due to improved lithium-ion diffusion. The improved NCM performance can therefore be attributed to the physical properties of the $LiAlO_2$ coating, particularly its superior lithium-ion conductivity. Moreover, the EIS of an increased $LiAlO_2$ coating content was performed on NMC (Fig. S4). Our results indicate that as a coating material of NMC, utilization of an ultrathin lithium-ion conductive $LiAlO_2$ significantly reduces the

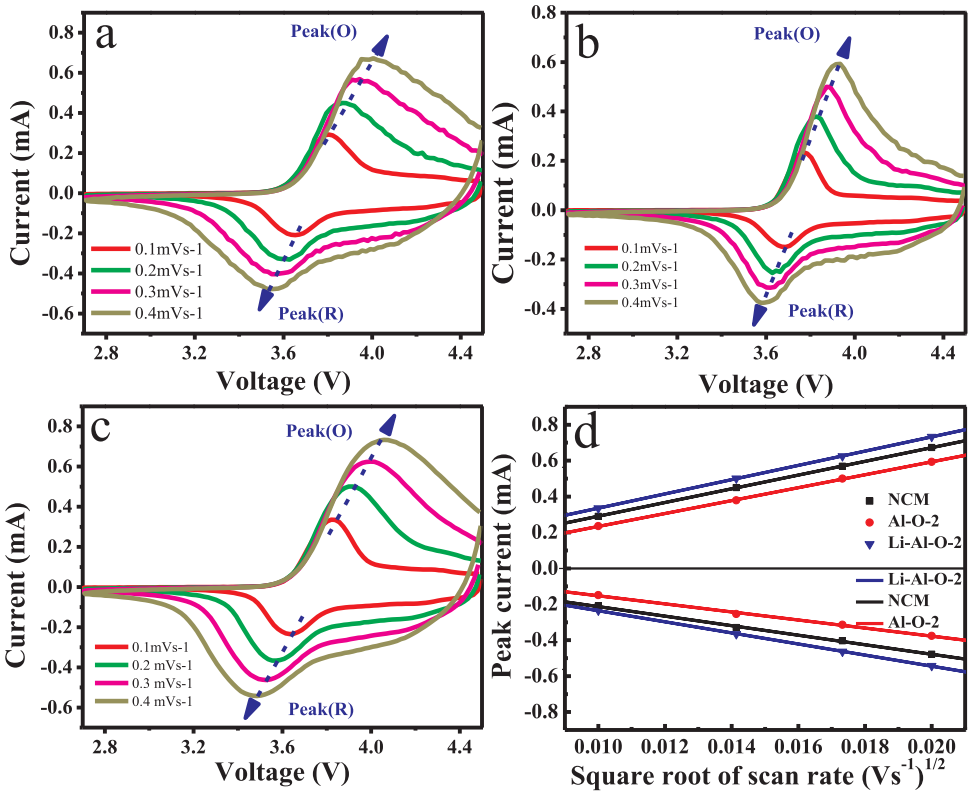

Fig. 9. CV curves of (a) NCM, (b) Al-O-2 and (c) Li-Al-O-2 at various scan rates; (d) the relationship of the peak current (i_p) and the square root of scan rate ($v^{1/2}$).

Table 1
The lithium-ion diffusion coefficients of NCM, Al-O-2 and Li-Al-O-2.

D_{Li}^+ ($cm^2\ s^{-1}$)	Li-insertion	Li-extraction
NCM	6.58×10^{-12}	3.17×10^{-12}
Al-O-2	5.84×10^{-12}	2.26×10^{-12}
Li-Al-O-2	7.12×10^{-12}	4.30×10^{-12}

Table 2
Electrochemical resistance of NMC, Al-O-2 and Li-Al-O-2 at various cycle.

Cycle number	1st cycle (4 V vs Li/Li^+)				30th cycle (4 V vs Li/Li^+)			
	R_s	R_f	R_{ct}	R_{f+ct}	R_s	R_f	R_{ct}	R_{f+ct}
NCM	3.007	97.5	83.65	181.15	3.226	305.7	143.7	449.4
Al-O-2	3.246	52.95	68.61	121.56	3.77	225.8	56.66	283.46
Li-Al-O-2	3.363	33.84	37.31	71.15	3.623	91.5	57.7	149.2

interfacial resistance between the cathode and electrolyte. To further support our conjecture, the surface morphologies of NCM, Al-O-2, and Li-Al-O-2 after 100 charge/discharge cycles at a cutoff voltage of 4.7 V are shown in Fig. S5. As opposed to the pristine morphology in Fig. 2a, small cracks can be observed on the surface of the cycled NCM (Fig. S5a). In contrast to NCM, both Al-O-2 and Li-Al-O-2 morphologies exhibit a relatively small change (Fig. S5b and c). At the primary particle surface, under HF acid etching during phase transformation, the

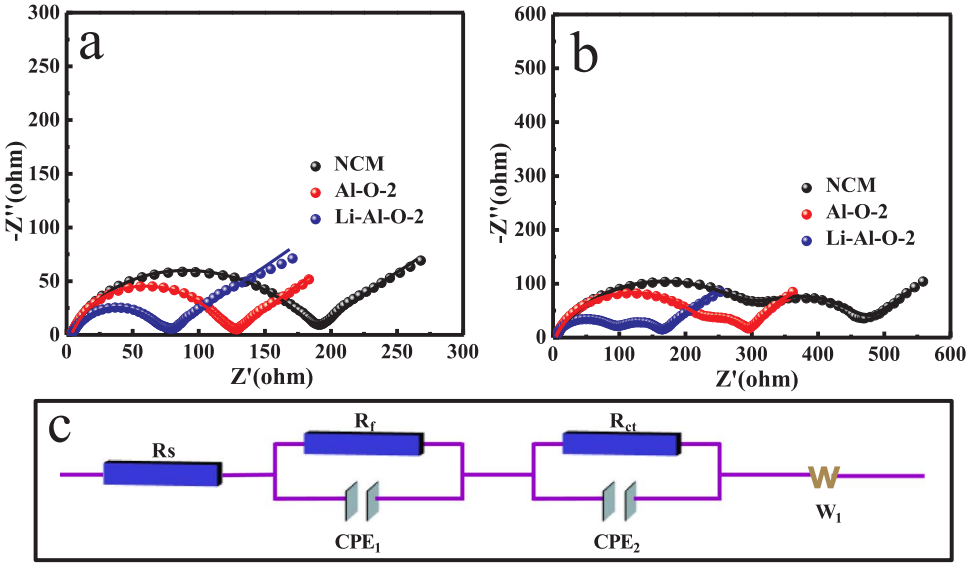

Fig. 10. Nyquist plots and fitting data of NCM, Al-O-2, and Li-Al-O-2 electrodes with an amplitude of 5.0 mV over a frequency range of 100 kHz to 0.01 Hz in the discharged state of 4.0 V: (a) in the 1st cycle; (b) in the 30th cycle; (c) the equivalent circuit.

structural degradation of the NCM cathode is triggered by evolution and the slow surface dissolution of the transition metal ions [13,17]. The results confirm that the Al_2O_3 and $LiAlO_2$ coatings are effective in improving the interface stability between the electrode active materials and electrolytes owing to protection of the NCM electrode from structural degradation during cycling.

4. Conclusions

Ultra-thin $LiAlO_2$ films with enhanced ionic conductivity were successfully designed and coated onto NCM via a sol-gel process , and their effect, compared to non-ionic conductive Al_2O_3 interfacial coatings, was investigated. Both coatings addressed the limitations exhibited by NCM, such as structural instability, dissolution of metal ions, and decomposition of the electrolyte. Compared to the Al_2O_3 coatings, however, the controllable and ultra-thin $LiAlO_2$ coating can be more effective in improving the cycling stability and rate capability of the NCM cathodes. This was attributed to the signification stabilization of the average discharge voltage especially at high cutoff voltages and current densities, as well as better lithium-ion transfer at the engineered interfaces. Therefore, this work demonstrates that the utilization of lithium-ion conducting films provides avenues of opportunity for building high performance cathode materials for LIBs.

Acknowledgments

This research was supported by the National Natural Science Foundation of China (51572194 and 51672189), The Key Project of the Tianjin Science & Technology Support Program (17YFZCGX00550), and Academic Innovation Funding of Tianjin Normal University (52XC1404).

Appendix A. Supplementary material

Supplementary data associated with this article can be found in the online version at http://dx.doi.org/10.1016/j.nanoen.2017.11.010.

References

[1] B. Dunn, H. Kamath, J.M. Tarascon, Science 334 (2011) 928–935.
[2] J.-M.T.M. Armand, Nature 414 (2001) 359–367.
[3] F. Wu, H. Zhou, Y. Bai, H. Wang, C. Wu, ACS Appl. Mater. Interfaces 7 (2015) 15098–15107.
[4] Y. Li, C. Wu, Y. Bai, L. Liu, H. Wang, F. Wu, N. Zhang, Y. Zou, ACS Appl. Mater. Interfaces 8 (2016) 18832–18840.
[5] Y. Li, Y. Bai, X. Bi, J. Qian, L. Ma, J. Tian, C. Wu, F. Wu, J. Lu, K. Amine, ChemSusChem 9 (2016) 728–735.
[6] Y. Bai, Y. Li, C. Wu, J. Lu, H. Li, Z.L. Liu, Y.X. Zhong, S. Chen, C.Z. Zhang, K. Amine, F. Wu, Energy Technol.-Ger. 3 (2015) 843–850.
[7] Y. Li, Y. Bai, C. Wu, J. Qian, G. Chen, L. Liu, H. Wang, X. Zhou, F. Wu, J. Mater. Chem. A 4 (2016) 5942–5951.
[8] P. Dong, D. Wang, Y. Yao, X. Li, Y. Zhang, J. Ru, T. Ren, J. Power Sources 344 (2017) 111–118.
[9] Z. Zheng, X.-D. Guo, S.-L. Chou, W.-B. Hua, H.-K. Liu, S.X. Dou, X.-S. Yang, Electrochim. Acta 191 (2016) 401–410.
[10] T. Li, X. Li, Z. Wang, H. Guo, J. Power Sources 342 (2017) 495–503.
[11] S.H. Cui, Y. Wei, T.C. Liu, W.J. Deng, Z.X. Hu, Y.T. Su, H. Li, M.F. Li, H. Guo, Y.D. Duan, W.D. Wang, M.M. Rao, J.X. Zheng, X.W. Wang, F. Pan, Adv. Energy Mater. 6 (2016) 1501309.
[12] Z. Huang, Z. Wang, X. Zheng, H. Guo, X. Li, Q. Jing, Z. Yang, Electrochim. Acta 182 (2015) 795–802.
[13] J. Xu, F. Lin, M.M. Doeff, W. Tong, J. Mater. Chem. A 5 (2017) 874–901.
[14] J. Lee, A. Urban, X. Li, D. Su, G. Hautier, G. Ceder, Science 343 (2014) 519–522.
[15] N.Y. Kim, T. Yim, J.H. Song, J.-S. Yu, Z. Lee, J. Power Sources 307 (2016) 641–648.
[16] H. Wang, W. Ge, W. Li, F. Wang, W. Liu, M.Z. Qu, G. Peng, ACS Appl. Mater. Interfaces 8 (2016) 18439–18449.
[17] X. Li, J. Liu, M.N. Banis, A. Lushington, R. Li, M. Cai, X. Sun, Energy Environ. Sci. 7 (2014) 768–778.
[18] S.H. Ju, I.S. Kang, Y.S. Lee, W.K. Shin, S. Kim, K. Shin, D.W. Kim, ACS Appl. Mater. Interfaces 6 (2014) 2546–2552.
[19] H. Kim, M.G. Kim, H.Y. Jeong, H. Nam, J. Cho, Nano Lett. 15 (2015) 2111–2119.
[20] F. Schipper, M. Dixit, D. Kovacheva, M. Talianker, O. Haik, J. Grinblat, E.M. Erickson, C. Ghanty, D.T. Major, B. Markovsky, D. Aurbach, J. Mater. Chem. A 4 (2016) 16073–16084.
[21] Y. Li, R. Xu, Y. Ren, J. Lu, H.M. Wu, L.F. Wang, D.J. Miller, Y.K. Sun, K. Amine, Z.H. Chen, Nano Energy 19 (2016) 522–531.
[22] S. Xu, R.M. Jacobs, H.M. Nguyen, S. Hao, M. Mahanthappa, C. Wolverton, D. Morgan, J. Mater. Chem. A 3 (2015) 17248–17272.
[23] W. Cho, S.-M. Kim, J.H. Song, T. Yim, S.-G. Woo, K.-W. Lee, J.-S. Kim, Y.-J. Kim, J. Power Sources 282 (2015) 45–50.
[24] F. Tao, X.-x. Yan, J.-J. Liu, H.-L. Zhang, L. Chen, Electrochim. Acta 210 (2016) 548–556.
[25] F. Wu, J. Tian, Y. Su, Y. Guan, Y. Jin, Z. Wang, T. He, L. Bao, S. Chen, J. Power Sources 269 (2014) 747–754.
[26] X. Li, J. Liu, X. Meng, Y. Tang, M.N. Banis, J. Yang, Y. Hu, R. Li, M. Cai, X. Sun, J. Power Sources 247 (2014) 57–69.
[27] J.-Z. Kong, C. Ren, G.-A. Tai, X. Zhang, A.-D. Li, D. Wu, H. Li, F. Zhou, J. Power Sources 266 (2014) 433–439.
[28] K. Liu, G.-L. Yang, Y. Dong, T. Shi, L. Chen, J. Power Sources 281 (2015) 370–377.
[29] Y. Su, S. Cui, Z. Zhuo, W. Yang, X. Wang, F. Pan, ACS Appl. Mater. Interfaces 7 (2015) 25105–25112.
[30] Y.P. Chen, Y. Zhang, F. Wang, Z.Y. Wang, Q. Zhang, J. Alloy. Compd. 611 (2014) 135–141.
[31] K. Yang, L.-Z. Fan, J. Guo, X. Qu, Electrochim. Acta 63 (2012) 363–368.
[32] W. Cho, S.M. Kim, K.W. Lee, J.H. Song, Y.N. Jo, T. Yim, H. Kim, J.S. Kim, Y.J. Kim, Electrochim. Acta 198 (2016) 77–83.
[33] J.S. Park, X. Meng, J.W. Elam, S. Hao, C. Wolverton, C. Kim, J. Cabana, Chem. Mater. 26 (2014) 3128–3134.
[34] K. Okada, N. Machida, M. Naito, T. Shigematsu, S. Ito, S. Fujiki, M. Nakano, Y. Aihara, Solid State Ion. 255 (2014) 120–127.
[35] Y. Hu, A. Ruud, V. Miikkulainen, T. Norby, O. Nilsen, H. Fjellvåg, RSC Adv. 6 (2016) 60479–60486.
[36] J. Rahn, E. Witt, P. Heitjans, H. Schmidt, Z. Phys. Chem. 229 (2015) 1341–1350.
[37] L. Li, Z. Chen, Q. Zhang, M. Xu, X. Zhou, H. Zhu, K. Zhang, J. Mater. Chem. A 3 (2015) 894–904.
[38] D.-T. Nguyen, J. Kang, K.-M. Nam, Y. Paik, S.-W. Song, J. Power Sources 303 (2016) 150–158.
[39] N.V. Kosova, E.T. Devyatkina, V.V. Kaichev, J. Power Sources 174 (2007) 965–969.
[40] J.W. Kim, D.H. Kim, D.Y. Oh, H. Lee, J.H. Kim, J.H. Lee, Y.S. Jung, J. Power Sources 274 (2015) 1254–1262.
[41] Y. Chen, Y. Zhang, B. Chen, Z. Wang, C. Lu, J. Power Sources 256 (2014) 20–27.
[42] J. Tian, Y. Su, F. Wu, S. Xu, F. Chen, R. Chen, Q. Li, J. Li, F. Sun, S. Chen, ACS Appl. Mater. Interfaces 8 (2016) 582–587.
[43] B. Yan, M. Li, X. Li, Z. Bai, J. Yang, D. Xiong, D. Li, J. Mater. Chem. A 3 (2015) 11773–11781.
[44] S. Li, X. Li, Y. Li, B. Yan, X. Song, D. Li, Electrochim. Acta 244 (2017) 77–85.
[45] S. Li, X. Li, Y. Li, B. Yan, X. Song, L. Fan, H. Shan, D. Li, J. Alloy. Compd. 722 (2017) 278–286.
[46] Y. Bai, L. Zhao, C. Wu, H. Li, Y. Li, F. Wu, ACS Appl. Mater. Interfaces 8 (2016) 2857–2865.

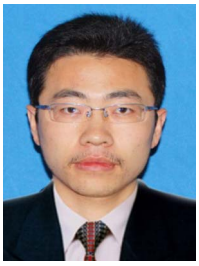

Wen Liu is currently a graduate student in the College of Physics and Materials Science, Tianjin Normal University. He received his BS degree from College of Chemistry and Materials Science, Shanxi normal University in 2015. His research is focus on the design and synthesis of novel nanomaterials for lithium and sodium ion batteries.

Xifei Li is currently a full professor at Tianjin Normal University and Xi'an University of Technology. Since 2001 he has been focusing on various materials for energy storage and conversion. Prof. Li's research group is currently working on design, synthesis as well as performance improvement of the anodes and the cathodes with various structures for high performance lithium ion batteries, lithium sulfur batteries, sodium ion batteries, and supercapacitors. He has authored and co-authored over 150 refereed journal articles with 5000 citations, two invited book chapters as well as 13 patents.

Dongbin Xiong is currently a Ph.D. candidate in the School of Materials Science and Technology at China University of Geosciences (Beijing). He received his Bachelor's degree (2012) and Master's degree (2016) from Wuhan University of Science and Technology (China) and Tianjin Normal University (China), respectively. His major research interests include the design and synthesis of novel nanomaterials for energy conversion and storage devices, especially for lithium ion batteries and supercapacitors.

Youchen Hao received his B.D. degree in School of Chemical Engineering, Anhui University of Science and Technology in 2015. He is currently pursuing his M.S. degree at the College of Physics and Materials Science, Tianjin Normal University. His research interests focus on nanomaterials for sodium ion batteries and lithium-sulfur batteries.

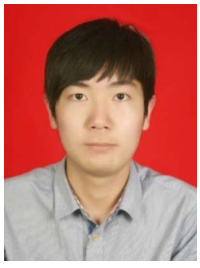

Jianwei Li received his B.D. degree in School of Physics and Materials Science, Ludong University in 2015. He is currently pursuing his M.S. degree at the College of Physics and Materials Science, Tianjin Normal University. His research interests focus on high performance electrode materials and their applications in supercapacitors and sodium ion batteries.

Huari Kou is currently a graduate student in the College of Physics and Materials Science, Tianjin Normal University. He received his BS degree from College of Science, Xi'an Jiaotong University in 2015. His research is focus on atomic layer deposition and sodium ion battery materials.

Bo Yan is currently an associate professor in the School of Materials Science and Technology at Xi'an University of Technology. He received his Ph.D. degree (2017) in the School of Materials Science and Technology at China University of Geosciences (Beijing). He received his M.E. (2014) and B.E. (2011) degree from the College of Chemistry and Bioengineering at Guilin University of Technology (Guilin, China). His current research interests focus on the controllable preparation of micro/nanostructures and their applications in lithium/sodium ion batteries and lithium-sulfur batteries.

Dejun Li is currently a full professor at Tianjin Normal University. He obtained his Ph.D. at Tsinghua University in 1999. He then worked three years as a postdoctoral follow at Northwestern University of USA. Since 1999 he has been focusing on various thin films, coatings, and nanomaterials for protection, energy storage and conversion. His research group is currently working on design, synthesis, and applications of various coatings for surface modification of the electrodes of various high performance batteries and supercapacitors as well as tools. He has authored and co-authored over 150 refereed journal articles and 11 patents.

Shigang Lu received his Ph.D. in chemistry from Moscow State University in 2003. He then worked as a postdoctoral fellow in Wuhan University and University of Science and Technology Beijing, respectively. At present, he is a professor of General Research Institute for Nonferrous Metals of China, and a director of China Automotive Battery Research Institute. His research expertise is in electrochemistry and its applications (lithium ion batteries, fuel cells, and molten salt electrolysis). He currently undertakes the research tasks of next-generation high energy density batteries.

Alicia Koo is a M.E.Sc. candidate in the Department of Mechanical and Materials Engineering at the University of Western Ontario. Her research focus is on the development of clean energy storage systems, particularly the design of nanomaterials with applications to batteries.

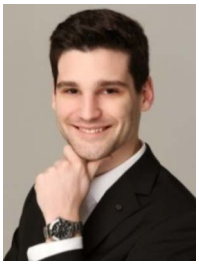

Keegan Adair received his B.Sc. in chemistry from the University of British Columbia in 2016. He is currently a Ph.D. candidate in Prof. Xueliang (Andy) Sun's Nanomaterials and Energy Group at the University of Western Ontario, Canada. Keegan has previously held multiple internships in the battery industry including positions at E-One Moli Energy and General Motors R&D. His research interests include the design of nanomaterials for lithium-ion batteries and nanoscale interfacial coatings for battery applications.

Professor Xueliang Sun is a Senior Canada Research Chair (Tier 1) and Full Professor at the University of Western Ontario, Canada. Dr Sun received his Ph.D. in 1999 at the University of Manchester, UK, which he followed up by working as a postdoctoral fellow at the University of British Columbia, Canada and as a Research Associate at l'Institut national de la recherche scientifique (INRS), Canada. His current research interests are associated with advanced materials for electrochemical energy storage and conversion, including electrocatalysis and catalyst support in fuel cells and electrodes in lithium-ion batteries and metal–air batteries.